

# Universal ferroelectric switching dynamics of vinylidene fluoride-trifluoroethylene copolymer films

Hu, Wei Jin; Juo, Deng-Ming; You, Lu; Wang, Junling; Chen, Yi-Chun; Chu, Ying-Hao; Wu, Tom

2014

Hu, W. J., Juo, D.-M., You, L., Wang, J., Chen, Y.-C., Chu, Y.-H., et al. (2014). Universal Ferroelectric Switching Dynamics of Vinylidene Fluoride-trifluoroethylene Copolymer Films. *Scientific Reports*, 4, 4772-.

<https://hdl.handle.net/10356/104112>

<https://doi.org/10.1038/srep04772>

---

This work is licensed under a Creative Commons Attribution-NonCommercial- NoDerivs 3.0 Unported License. The images in this article are included in the article's Creative Commons license, unless indicated otherwise in the image credit; if the image is not included under the Creative Commons license, users will need to obtain permission from the license holder in order to reproduce the image. To view a copy of this license, visit <http://creativecommons.org/licenses/by-nc-nd/3.0/>

*Downloaded on 25 Aug 2022 21:48:35 SGT*



OPEN

SUBJECT AREAS:  
ELECTRONIC DEVICES  
POLYMERS  
FERROELECTRICS AND  
MULTIFERROICS

# Universal Ferroelectric Switching Dynamics of Vinylidene Fluoride-trifluoroethylene Copolymer Films

Wei Jin Hu<sup>1</sup>, Deng-Ming Juo<sup>2</sup>, Lu You<sup>3</sup>, Junling Wang<sup>3</sup>, Yi-Chun Chen<sup>2</sup>, Ying-Hao Chu<sup>4</sup> & Tom Wu<sup>1</sup>Received  
7 November 2013Accepted  
1 April 2014Published  
24 April 2014Correspondence and  
requests for materials  
should be addressed to  
T.W. (Tao.Wu@kaust.  
edu.sa)

<sup>1</sup>Physical Sciences and Engineering Division, King Abdullah University of Science and Technology, Thuwal, 23955-6900, Saudi Arabia, <sup>2</sup>Department of Physics, National Cheng Kung University, Tainan 70101, Taiwan, <sup>3</sup>School of Materials Science and Engineering, Nanyang Technological University, Singapore 639798, Singapore, <sup>4</sup>Department of Materials Science and Engineering, National Chiao Tung University, Hsinchu 30010, Taiwan.

**In this work, switching dynamics of poly(vinylidene fluoride-trifluoroethylene) [P(VDF-TrFE)] copolymer films are investigated over unprecedentedly wide ranges of temperature and electric field. Remarkably, domain switching of copolymer films obeys well the classical domain nucleation and growth model although the origin of ferroelectricity in organic ferroelectric materials inherently differs from the inorganic counterparts. A lower coercivity limit of 50 MV/m and 180° domain wall energy of 60 mJ/m<sup>2</sup> are determined for P(VDF-TrFE) films. Furthermore, we discover in copolymer films an anomalous temperature-dependent crossover behavior between two power-law scaling regimes of frequency-dependent coercivity, which is attributed to the transition between flow and creep motions of domain walls. Our observations shed new light on the switching dynamics of semi-crystalline ferroelectric polymers, and such understandings are critical for realizing their reliable applications.**

Ferroelectric (FE) materials are extensively applied in a myriad of critical technologies such as nonvolatile random access memories, field-effect transistors, sensors, actuators and solar cells<sup>1–6</sup>. It is of great importance to understand the polarization switching dynamics which determines how fast such FE devices can operate<sup>7–10</sup>. Several groundbreaking models have been proposed to explain the diverse, even contradictory behaviors of switching dynamics reported in literature. The Kolmogorov-Avrami-Ishibashi (KAI) model, which assumes the statistical formation of a large number of nucleation sites and homogeneous domain growth, is satisfactory for describing uniformly polarized single crystals and epitaxial films<sup>11–13</sup>. On the other hand, in the nucleation-limited-switching (NLS) model, the region-by-region nucleation and switching are the dominant factors, and this model is usually used to explain the relatively slow switching in some ferroelectric thin films<sup>14–16</sup>. Recently, in order to account for the switching kinetics in a wide temperature range for disordered PbZr<sub>1-x</sub>Ti<sub>x</sub>O<sub>3</sub> (PZT) films, Jo et al. considered the inhomogeneous strength of local electric field and developed a Lorentzian distribution model for the switching time<sup>17</sup>. A similar inhomogeneous field mechanism (IFM) was proposed to explain the temporal FE behavior of virgin and fatigued PZT ceramics<sup>18</sup>.

Compared to the inorganic counterparts, the switching dynamics of organic FE materials has been much less investigated. Besides respectable piezoelectric and pyroelectric properties, FE polymers such as polyvinylidene fluoride (PVDF) are low-cost, lightweight, flexible, environment-friendly (lead-free) and easily processable<sup>19,20</sup>. They have the potential to be employed in modern applications, in particular novel memory devices and transducers<sup>21–24</sup>. In addition, phenomena like two-dimensional ferroelectricity have been claimed for ultrathin PVDF films<sup>25</sup>. As a result of different chain conformations, the polymer presents five crystalline phases, i.e.,  $\alpha$ ,  $\beta$ ,  $\gamma$ ,  $\delta$  and  $\epsilon$ , which is extensively discussed in a recent review<sup>26</sup>. Among the phases, the FE  $\beta$  phase has an all trans (TTT) planar zigzag conformation (Fig. 1a) and the largest dipole moment. Copolymer with Trifluoroethylene [P(VDF-TrFE)] is one of the approaches to promote the formation of FE  $\beta$  phase. Different from the ceramic FE materials like BaTiO<sub>3</sub> where ionic displacement produces polarization, the FE order of PVDF polymer and P(VDF-TrFE) copolymers, is originated from the permanent dipoles and the cooperative long-range rotation of the molecular chains via the short-range van der Waals interactions (Fig. 1a and b)<sup>27,28</sup>. Another difference is

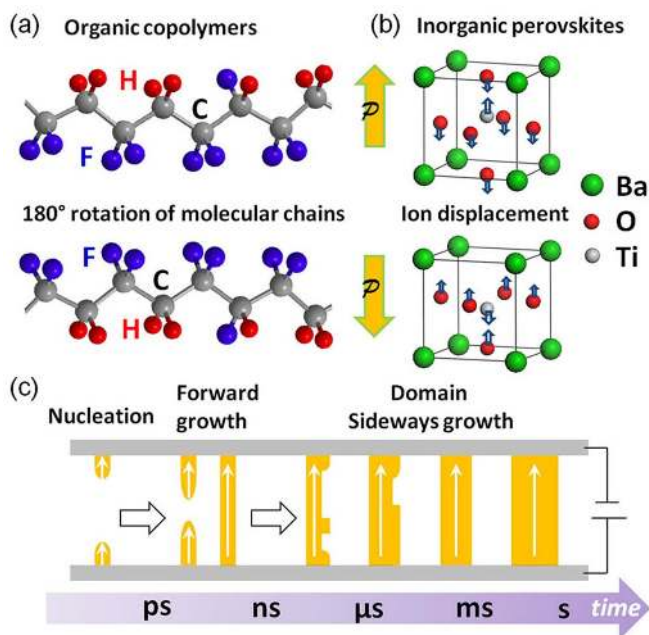


**Figure 1** | Comparison of microscopic origin of polarization switching in organic and inorganic FE materials. (a) Schematic molecular structure and FE switching of P(VDF-TrFE) polymer. (b) Switching mechanism of a typical inorganic perovskite BaTiO<sub>3</sub>. (c) Universal polarization switching process involves nucleation, forward domain growth and sideways domain growth through kink nucleation, spanning many time scales.

the semi-crystalline nature of this polymer which is known for the ubiquitous presence of amorphous phase in addition to the ferroelectric crystalline phase<sup>26,27</sup>. These distinctive characters of PVDF polymers are expected to impact the switching dynamics, and whether the above mentioned models which were developed for inorganic FE materials is applicable for polymers poses as an intriguing question.

At present, the switching mechanism in PVDF and its copolymers remains as an unsolved issue, and the reports in literature are often contradictory to each other. Recently, Mao et al. claimed that the switching dynamics in the P(VDF-TrFE) films can be described by the NLS model<sup>29</sup>. In another study based on piezoresponse force microscopy (PFM), Gysel et al. proposed that the restricted domain growth appears to follow a non-KAI mechanism<sup>30</sup>. On the other hand, Schütrumpf et al. argued that the IFM model is applicable to

the two-stage switching behavior observed in the thick P(VDF-TrFE) films<sup>31</sup>. The fact that the time scale of ferroelectric switching dynamics is extremely broad, expanding many orders of magnitudes, makes the unambiguous determination of the underlying mechanism rather challenging. As illustrated in Figure 1c, the universal polarization switching process microscopically involves the nucleation, the forward domain growth and the subsequent sideways growth. The timescale for nucleation and forward domain growth is typically 1 ps to 1 ns, whereas for sideways domain growth it is from several nanoseconds to seconds or even longer depending on various intrinsic and extrinsic factors. Furthermore, defects and structural disorders introduced during synthesis, can significantly influence the switching dynamics in P(VDF-TrFE) films by acting as nucleation centers and pinning sites for the domain wall motion, further escalating the complexity of the process.

In this work, we systematically investigated the switching dynamics of P(VDF-TrFE) films at varying temperatures in an unprecedentedly wide frequency range from 0.002 Hz to 100 kHz. Our data suggest that the classical KAI model based on nucleation and unrestricted growth of ferroelectric domains is applicable to organic FE materials, similar to the ceramic counterparts. Furthermore, we observed in our copolymer films a hitherto unreported crossover phenomenon between two different scaling regimes of frequency-dependent polarization switching. Besides the macroscopic switching experiments, we used the complementary PFM technique to explore the nanoscale spatially resolved polarization dynamics in P(VDF-TrFE) films. Our measurement results covering wide time and space scales reveal the persistence of the universal scaling law of phase transformation in copolymer thin films, and the robust switching with determined thermodynamic parameters like domain wall energy and lower limit of coercivity facilitates the reliable applications of such organic materials.

## Results

**Structural characterization.** Figure 2a shows the XRD data of the spin-coated P(VDF-TrFE) films on Cu(Pt)(100 nm)/Ti(10 nm)/Si(100) substrates. The diffraction peak at  $2\theta = 19.7^\circ$  is characteristic of the (200) and (110) crystalline planes of the ferroelectric  $\beta$  phase<sup>26,28</sup>. Figure 2b shows the AFM image of a 510 nm polymer film deposited on the Pt substrate, and the RMS roughness is about 27 nm. Large grains with a size of  $\sim 1\text{--}2\ \mu\text{m}$  are observed, and the close-up view in the inset suggests that the grains are composed of needle-like crystallites with a thickness of  $\sim 100\ \text{nm}$  and length of 100–300 nm. Such morphology is characteristic of the ferroelectric  $\beta$  phase<sup>28</sup>, consistent with the XRD result. Similar XRD and AFM

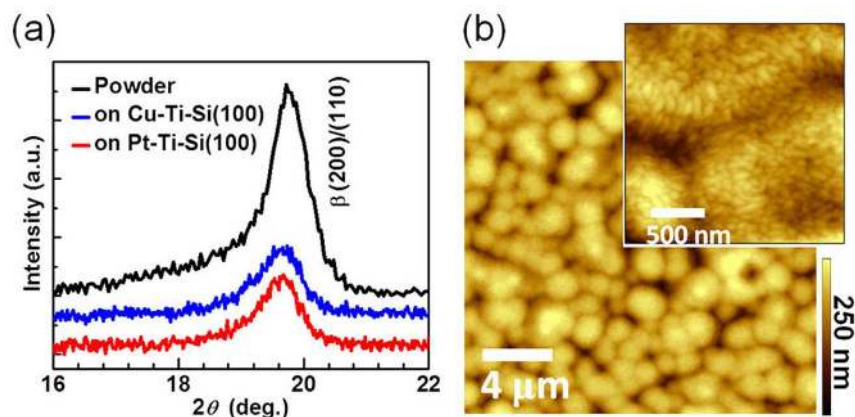


**Figure 2** | Structural and morphology characterization. (a) XRD curves of the precursor powder and the spin-coated films on Cu(Pt)/Ti/Si(100) substrates; (b) AFM image obtained from the 510 nm P(VDF-TrFE) film after annealing at 140°C for 2 hours. Inset in (b) is the enlarged image showing the aggregated needle-like ferroelectric  $\beta$  crystallites.



results were obtained for polymer films coated on Cu-coated substrates, suggesting that different metal surfaces have negligible effect on the structure and morphology of the P(VDF-TrFE) films.

**Scaling law behaviors of coercivity over frequency.** To investigate the frequency dependence of the FE switching dynamics,  $P$ - $E$  loops were measured using triangular-shaped voltage pulses with different frequencies applied onto the capacitors. The high quality of the films is verified by the small leakage current, allowing us to investigate the polarization switching behavior in a wide frequency range (i.e., from 0.05 Hz to 100 kHz). Shown in Figure 3a are the  $P$ - $E$  loops measured at 300 K. As the frequency decreases, there is an obvious decrease of the coercivity ( $E_c = (E_{c+} - E_{c-})/2$ , defined as the half width of the  $P$ - $E$  loop where it crosses the  $E$  axis) in the high frequency range (100 Hz to 100 kHz), whereas the change is negligible in the low frequency range (below 100 Hz). These frequency-dependent behaviors suggest two different regimes of switching dynamics. Note that as the applied electric field is much bigger than the coercivity at the measurement temperatures, artifacts associated with the incomplete saturation of polarization are avoided. The remanent polarization ( $P_r$ ) remains almost constant, also indicating the saturation of the  $P$ - $E$  loops. The values of  $P_r \sim 8 \mu\text{C}/\text{cm}^2$  and  $E_c \sim 60 \text{ MV}/\text{cm}$  measured at 1 Hz are consistent with those reported for spin-coated P(VDF-TrFE) films<sup>28,32</sup>. The measurement temperature also significantly affects the  $P$ - $E$  hysteresis loops. Figure 3b shows the  $P$ - $E$  loops at 0.1 Hz measured from 350 K down to 100 K. Overall,  $E_c$  increases sharply on decreasing temperature, reaching  $\sim 180 \text{ MV}/\text{m}$  at 100 K, or about three times of that measured at 300 K.

To obtain further insights on the switching dynamics, we plot in Figure 3c  $\log E_c$  vs.  $\log f$  measured at different temperatures on a Cu/P(VDF-TrFE)/Cu capacitance device. For ferroelectric switching through nucleation and unrestricted domain growth, a simple power

law was theoretically predicted and experimentally confirmed for several inorganic ferroelectric materials<sup>12,33,34</sup>. In this nucleation-limited scenario, the frequency-dependent coercivity follows  $E_c \sim f^\beta$ , which fits the data of P(VDF-TrFE) film very well (the solid lines in Fig. 3c). Interestingly, at temperatures above 250 K we observed two different scaling behaviors for the low frequency and the high frequency regimes separated by a crossover frequency  $f_{cr}$ . This crossover phenomenon was also observed in devices with other electrode combinations of Pt/Pt and Pt/Cu, which suggests that this phenomenon is correlated with the intrinsic properties of P(VDF-TrFE) polymer films. Such a crossover phenomenon was previously observed in PZT films<sup>12,33,34</sup>, but it has not been reported for any organic FE material. It is remarkable that our polymer samples share this property with the ceramic FE counterparts. As a unique feature, the crossover frequency  $f_{cr}$  in our polymer films shifts to lower values on decreasing temperature, and at temperatures below  $\sim 200 \text{ K}$  the crossover disappears in the frequency range investigated. This temperature-dependent behavior is different from the report on PZT films where  $f_{cr}$  remains nearly constant in a wide range of temperature<sup>33</sup>.

Originally, such  $E_c$ - $f$  crossover phenomena were reported for ferromagnetic systems, and they were qualitatively explained by the nucleation and propagation of domain walls<sup>35-37</sup>. The crossover was proposed to correlate with the competition and transformation of thermally activated domain wall motion (creep) and viscous displacement (flow) of domain walls<sup>35,38</sup>. Recently, Yang and coworkers extended such models to explain the crossover phenomenon observed in ferroelectric PZT films, and they proposed that there exists a crossover between domain wall creep and flow regimes<sup>33</sup>. The crossover electric field  $E_{cr}$  can be written as,

$$E_{cr}/E_{c0} = [(U/k_B T)(1 - E_{cr}/E_{c0})^\eta]^{1/\mu} \quad (1)$$

where  $E_{c0}$  is the depinning electric field at  $T = 0 \text{ K}$ ,  $U$  is the pinning energy barrier,  $\eta = 2$  is the exponent related to the  $E$  dependence of

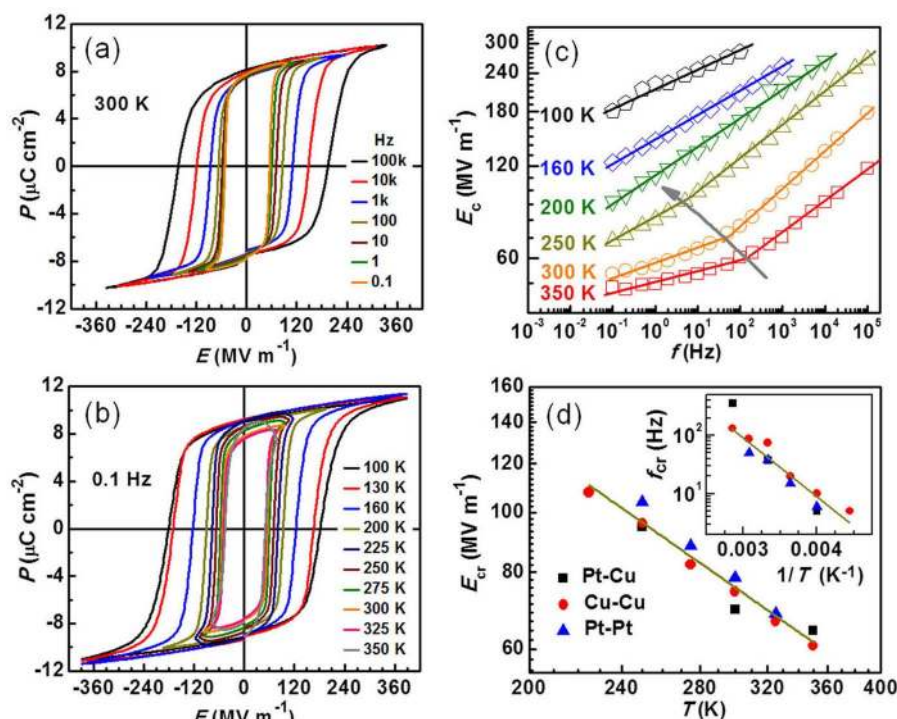


**Figure 3 | Ferroelectric hysteresis loops for the Cu/P(VDF-TrFE)/Cu capacitor-type device and scaling behaviors of coercivity  $E_c$  over frequency  $f$ .** (a)  $f$ -dependent  $P$ - $E$  loops at 300 K. (b) Temperature-dependent  $P$ - $E$  loops at 0.1 Hz. (c)  $f$ -dependent  $E_c$  at different temperatures. The solid line is the power law fitting as discussed in the main text. The grey arrow highlights the temperature-dependent crossover frequencies between two different power-law regimes. (d) Double logarithmic plot of crossover coercive field  $E_{cr}$  vs. temperature  $T$  measured on three devices. Inset shows the crossover frequency  $f_{cr}$  as a function of the inverse temperature. The straight solid lines indicate the fitting results as discussed in the main text.



energy barrier, and  $\mu$  is the dynamic exponent which is determined by the type of disorder. Since  $E_{cr}$  is much smaller than  $E_{c0}$  at high temperatures, we can rewrite Equation (1) as,

$$\log E_{cr} = A - (1/\mu) \log T, \quad (2)$$

where the constant  $A = \log E_{c0} + (1/\mu) \log(U/k_B)$ .

Figure 3d shows the data of temperature dependent  $E_{cr}$  measured on three different devices and the fitting result according to Equation (2). The good match between data and model indicates that the observed crossover behavior may originate from the transition between regimes of domain creep and viscous flow. Furthermore, we derived  $\mu = 0.76(5)$ . Note that the value of  $\mu$  reflects the nature of disorders in the system, which pin the domain walls and affect their dynamics. In the random-bond scenario, defects modify the FE double-well potential symmetrically and  $\mu = 0.5$ – $0.6$  for a 2D domain wall<sup>40</sup>. For the random-field case, defects induce asymmetric change to the double well and  $\mu = 1$ . The former is based on the short-range elastic interactions induced by neutral defects, while the latter considers the long-range interactions such as the electrostatic force induced by charged defects. The value estimated above suggests that the random-bond disorders are dominant in the P(VDF-TrFE) polymer, which is consistent with the neutral nature of defects due to chain conformation and miss-packing<sup>39</sup>. This is different from the case of FE ceramics such as PZT, where charged defects such as oxygen vacancies conform better to the random-field scenario, leading to  $\mu = 0.9$  as reported recently<sup>17,33,40</sup>. In addition, the shift of  $f_{cr}$  on reducing temperature reflects the thermal activation nature of the domain creep, which can be expressed as  $f_{cr} \sim \tau_0^{-1} \exp(-U_B(E_{cr})/k_B T)$ <sup>33</sup>. In this expression,  $\tau_0$  and  $U_B(E_{cr})$  are the characteristic time and the energy barrier of domain creep, respectively. Indeed, as shown in the inset of Figure 3d, the data of  $f_{cr}$  exhibits such a thermal activation behavior, and the fitting yields  $\tau_0 \sim 5 \times 10^{-6}$  s and  $U_B(E_{cr})/k_B \sim 1109(115)$ .

**Lower limit of coercivity.** Whether there exists a lower limit of coercivity at very low  $f$  is a fundamental question for ferroelectrics. It is usually difficult to draw conclusions because at low frequencies the electronic current may exceed the polarization-switching current, which makes it very hard to determine the FE coercivity. According to the continuum theory which was developed to describe heterogeneous transformation and thermal growth processes, there exists a lower limit for  $E_c$  as the switching barrier<sup>41</sup>. On the other hand, the random-field model states that switching could occur even under a very small electric field through the nucleation of polar clusters<sup>42</sup>. Experimental results on  $0.955\text{Pb}(\text{Zn}_{1/3}\text{Nb}_{2/3})\text{O}_3$ – $0.045\text{PbTiO}_3$  (PZN-4.5% PT) single crystals using an ultrasonic technique suggest the existence of a lower limit of  $E_c$ , and seem to favor the continuum theory<sup>43</sup>. On the other hand, experiments on  $0.7\text{Pb}(\text{Mn}_{1/3}\text{Nb}_{2/3})\text{O}_3$ – $0.3\text{PbTiO}_3$  (PMN-PT 70/30) polycrystalline soft ferroelectrics support the random-field model<sup>42</sup>. However, this issue has not been discussed in the context of organic FE polymers. To determine the low- $f$  coercivity, we carried out the quasi-static  $I(V)$  measurements and derived the  $P$ - $E$  loops of the P(VDF-TrFE) films through the following equation,

$$P = \frac{Q}{A} = \frac{1}{A} \int_0^t Idt = \frac{1}{A} \frac{dV}{dV} \int_0^V IdV, \quad (3)$$

where  $P$  is the switched-polarization,  $A$  is the area of junction, and  $Q$  is the amount of charges associated with  $P$ . The coercivity  $E_c$  is determined from the calculated  $P$ - $E$  loops.

Figure 4a shows the switching  $I(V)$  curves with different sweeping rates measured on a Cu/P(VDF-TrFE) (286 nm)/Cu capacitor at 300 K. Two current peaks are observed and they correspond to the polarization switching of the P(VDF-TrFE) film. Furthermore, the peak current values decrease with increasing the sweeping period  $T$  from 28.5 s to 500 s (equivalent to reducing  $f = 1/T$  from 0.035 Hz

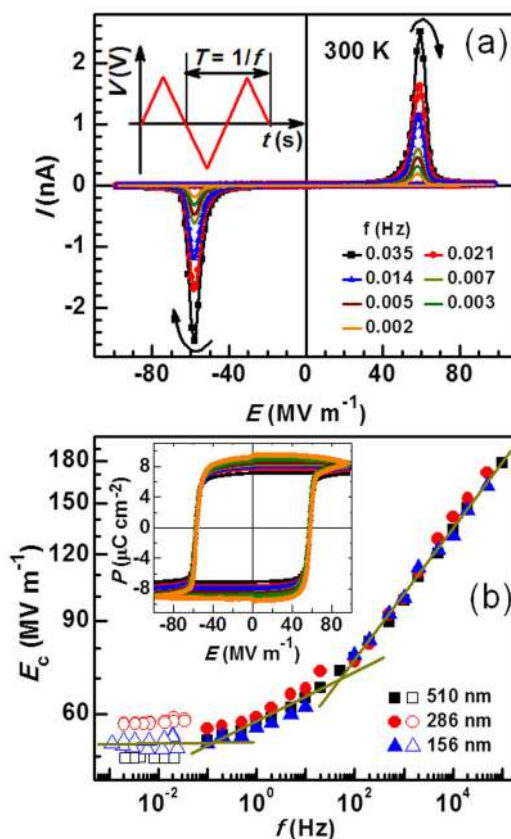


**Figure 4 | Determination of the lower limit of coercivity.** (a) Quasi-static  $I(V)$  curves measured with different sweeping periods at 300 K for the device of Cu/P(VDF-TrFE) (286 nm)/Cu. The calculated  $P$ - $E$  loops are shown in the inset of (b). (b)  $f$  dependence of  $E_c$  for three films with different thicknesses. The solid symbols represent the data derived from the  $P$ - $E$  loops, whereas the empty symbols represent the low-frequency data derived from the quasi-static  $I(V)$  curves.

to 0.002 Hz). The current peaks, on the other hand, show negligible horizontal shift in Figure 4a. This is also evidenced in the calculated quasi-static  $P$ - $E$  loops shown in the inset of Figure 4b, where all the  $P$ - $E$  loops overlap with each other, and  $P_r$  of  $\sim 8 \mu\text{C}/\text{cm}^2$  is consistent with the high- $f$  values shown in Figure 3a. To achieve reliable results on the  $f$  dependence of  $E_c$ , we investigated P(VDF-TrFE) devices with three different film thicknesses, and the data are shown in Figure 4b. In addition to the crossover phenomenon mentioned above, there exists a lower limit of  $E_c$  around 50 MV/m, and the exact value of the  $E_c$  limit shows a weak dependence on the film thickness. Therefore, our data appears to support the continuum theory; in other words, an intrinsic threshold switching barrier exists at very low frequencies for P(VDF-TrFE) films. It is note worthy that the nature of disorders in P(VDF-TrFE) copolymers is consistent with continuum theory since the random-bond elastic potential introduced by the neutral defects is one of the basic assumptions of the continuum theory<sup>42,43</sup>.

**KAI model as the universal switching mechanism for P(VDF-TrFE) films.** We further explored the switching kinetics by performing the PUND measurements at different temperatures on the Cu/P(VDF-TrFE) (510 nm)/Pt capacitor. In the PUND method, five sequential voltage pulses are applied on the device as shown in Figure 5a. The first negative pulse is used for resetting the polarization state, and the switching polarization ( $P^*$ ) is recorded during the end of the second pulse. The non-switching polarization ( $P^\wedge$ ) is measured during the third pulse, which contains only the non-remanent polarization.  $P_{sw} = P^* - P^\wedge$  is then the pure switching polarization that originates from

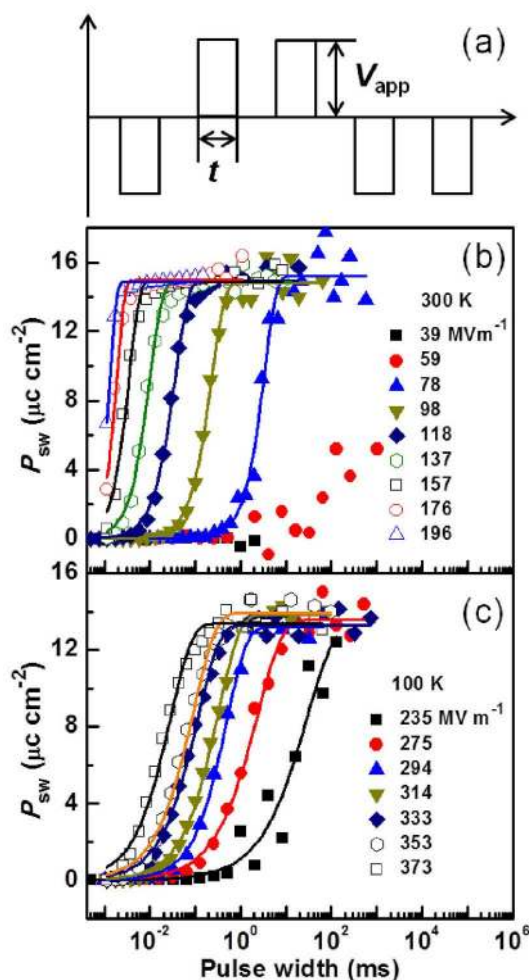


**Figure 5 | Dynamics of polarization switching.** (a) Pulse sequence used in the measurements of switching time.  $V_{app}$  and  $t$  are the magnitude and the width of the applied voltage pulses, respectively. The switching polarization  $P_{sw}$  versus the pulse width for different electric fields measured at (b) 300 K and (c) 100 K. The solid lines are fittings according to the KAI model as discussed in the text.

the FE component. Typical switching results at 300 K and 100 K are shown in Figure 5b and c, respectively. Depending on the applied electric field, the polarization switching occurs in a wide time range from  $10^{-6}$  to 1 s. We should note that the switching can be faster than  $10^{-6}$  s, but our measurements are limited by the equipment capability. Furthermore, the switching consistently occurs within a narrow time range of one decade and the polarization saturates quickly, which is different from the previous results reported for PVDF films<sup>29–31</sup>. This fast switching may be related to the homogeneous crystalline quality of our films. As shown in Figure 5b, at 300 K, the switching starts at  $E \sim 59$  MV/m, which is close to the coercivity measured in the low frequency range (Fig. 4b). Below 59 MV/m, we did not observe any switching in the time range investigated. As the temperature decreases to 100 K, much higher values of  $E$  are required for the switching, and the switching is also much slower than the 300 K case. This is expected because the rotation of the molecules and the movement of domain walls are retarded at low temperatures.

We found that the polarization switching of our PVDF films is similar to the behavior previously reported for high-quality epitaxial PZT films<sup>12,33</sup>, which can be well described by the KAI model<sup>11</sup>. This model, based on the assumption of homogeneous nucleation and unrestricted domain growth, states that,

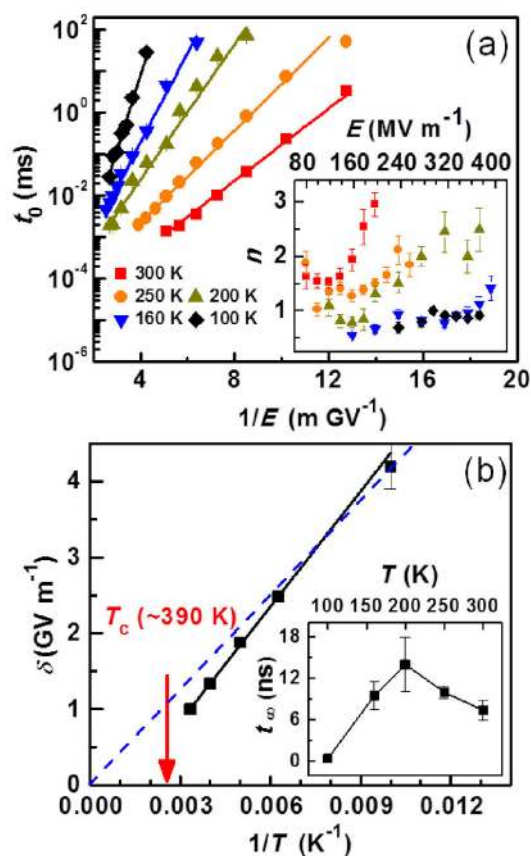


**Figure 6 | Fitting of polarization switching data to the KAI model.** (a) The characteristic switching time  $t_0$  vs.  $1/E$  at various temperatures. The solid lines are fittings according to the Mertz' law. Inset: the KAI model fitting parameter  $n$  vs.  $T$ . (b) Plot of the activation field  $\delta$  vs.  $1/T$ . The solid lines are fitting according to the domain nucleation model. The dashed line is guide for the eyes. Inset: Plot of  $t_\infty$  vs.  $T$ , showing a cusp around 200 K.

$$P_{sw}(t) = 2P_r[1 - \exp(-(t/t_0)^n)], \quad (4)$$

where  $t_0$  and  $n$  are the characteristic switching time and the geometric dimension for the domain growth, respectively. The solid lines in Figure 5 are the fitting curves, indicating that the experimental data can be well explained by the KAI model.

The fitting parameters in the Equation (4), including  $n$  and  $t_\infty$ , as functions of electric field and temperature, are shown in Figure 6a.  $n$  is known to be dependent on the nucleation rate of the opposite domains and the dimension of their growth. From the inset of Figure 6a, we found that  $n$  becomes larger on increasing  $E$  and reaches  $\sim 3$  at 300 K. This indicates that at high temperatures, the domain nucleation and growth is isotropic, i.e., the domains nucleate and propagate along many molecular chains simultaneously due to the strong inter-chain coupling. On the other hand,  $n$  remains almost constant at  $\sim 1$  below 160 K, which suggests weakened inter-chain coupling. Further insights could be obtained from the log scale plot of  $t_0$  vs  $1/E$ , as shown in Figure 6a. The linear relationship indicates that the characteristic switching time follows the empirical Mertz's law, i.e.,

$$t_0 = t_\infty \exp(\delta/E), \quad (5)$$

where  $t_\infty$  is the lower limit of switching time and  $\delta$  is the activation field<sup>44–46</sup>.  $\delta$  and  $t_\infty$  as derived from the fitting are shown in Figure 6b and the inset, respectively.  $\delta \sim 1.0$  GV/m at 300 K, which agrees well with other reports<sup>47</sup>. At a lower temperature of 100 K,  $\delta$  increases to 4.2 GV/m at 100 K. On the other hand,  $t_\infty$  shows nonmonotonous



temperature dependence with a peak of 14 ns at 200 K, indicating a subtle change of switching kinetics. At 100 K,  $t_{\infty}$  reaches a low value of 0.4 ns, which is one order smaller than the value reported for thinner PVDF films<sup>47</sup>.

Although the classical KAI model is usually considered for inorganic materials, our results suggest that it could also be applied to describe the FE switching of PVDF copolymers, where the ferroelectricity stems from the rotation of long molecule chains. In a previous theoretical report, it was proposed that the switching of PVDF occurs through the formation of kinks and their solitary propagation along the chain segments<sup>48</sup>. This is very similar to the Miller-Weinreich model initially proposed for BaTiO<sub>3</sub>, where the sideways motion of domain walls is controlled by the kink nucleation<sup>49,50</sup>. In the model, the critical triangular nucleus has a half-hemline length of  $a^*$  and a height of  $l^*$ . By ignoring the depolarization energy of the opposite domain nucleus, we can write the activation field in the Merz's equation and the critical nucleus size as follows,

$$\delta = c\sigma_w^2/P_s k_B T, \quad (6)$$

$$a^* = l^* = \sigma_w / \sqrt{2P_s E}, \quad (7)$$

where  $\sigma_w$  is the domain wall energy;  $P_s$  is the saturation polarization, which is  $\sim 13 \mu\text{C}/\text{cm}^2$  for 100% crystallized P(VDF-TrFE)<sup>51</sup>,  $c$  is the wall width or presumably the lattice constant along the chain ( $\sim 2.56 \text{ \AA}$ ). Eq. (6) suggests that  $\delta$  is linear proportional to  $1/T$  with the intersection across zero, which is shown as the dashed line in Figure 6b. When approaching to the Curie point ( $T_c \sim 390 \text{ K}$ )<sup>25</sup>, simultaneous multi-nucleation processes may be involved<sup>49</sup>, which decreases the energy barrier and induces a deviation of the data from the prediction of Equation 6, as shown in Figure 6b. Nevertheless, by assuming  $180^\circ$  domain walls moving along the low-index (110) chain planes, we can roughly estimate  $\sigma_w$  to be  $60 \text{ mJ}/\text{m}^2$ , which is comparable to the reported values in thin films of BaTiO<sub>3</sub> ( $3\text{--}17 \text{ mJ}/\text{m}^2$ )<sup>51</sup> and PbTiO<sub>3</sub> ( $132 \text{ mJ}/\text{m}^2$ )<sup>50</sup>. The critical energy barrier ( $U^* = c\sigma_w^2/P_s E$ ) is  $29 k_B T$  for  $E_c$  of  $59 \text{ MV}/\text{m}$  at  $300 \text{ K}$ , which is larger than that estimated for Langmuir-Blodgett PVDF thin films ( $\sim 15 k_B T$ )<sup>24</sup>, and within the range of values reported for inorganic FE materials like BaTiO<sub>3</sub> ( $40 k_B T$ )<sup>52</sup> and PZT ( $\sim 10 k_B T$ )<sup>33</sup>. The critical nucleus size ( $2a^* \times l^*$ ) is  $11 \times 5.5 \text{ nm}^2$  (at  $E_c$  of  $59 \text{ MV}/\text{m}$ ) at  $300 \text{ K}$  and decreases to  $3.2 \times 1.6 \text{ nm}^2$  (at  $E_c$  of  $206 \text{ MV}/\text{m}$ ) at  $100 \text{ K}$ . This suggests that much less numbers of chain segments are involved in individual nucleus at low temperatures, which is consistent with what we previously concluded from the temperature dependence of the geometric dimension  $n$ . However, we want to note that the above value of domain wall energy could be overestimated as this model does not consider the diffusive character of polarization charges across the walls<sup>50,53</sup>. Other extrinsic effects such as grain boundaries and defect-induced disorders could also affect the above estimation<sup>53</sup>.

**Local domain switching.** Recently, PFM has been proven to be a powerful technique to probe the relationship between polarization switching and local microstructure in FE materials<sup>54–58</sup>. To get further insight into the domain switching, we examined the nanoscale domain wall motion on a  $66 \text{ nm}$  P(VDF-TrFE)/Pt film by PFM. We used a thinner copolymer film here so that it can be switched by the voltage applied within the limit of PFM. The film has no top electrode, and voltage pulses were applied through a sharp Pt-coated PFM tip (radius  $\sim 20 \text{ nm}$ ) to locally induce switched nuclei and drive domain-wall motion. In the as-grown film, there are no clear features of domain structures. Based on the out-of-plane (OP) PFM phases, most as-grown regions are polarized downward, i.e., with polarizations toward the substrate. To study the upward and downward domain switching dynamics, the switching voltage pulses were applied on a large matrix previously poled downward

and upward, respectively. Figure 7a and c show OP PFM images of the domains formed by different voltage pulses. The dark region is downward polarized while the bright region is upward polarized, which is confirmed by the  $180^\circ$  PFM phase difference between two regions. The electric field from the tip decays with the distance from the tip, and  $E(r)$  has a  $1/r$  dependence to the first-order approximation. Unlike the macroscopic measurements, only one nucleation center of a switched domain is formed in the high-field region near the PFM tip. The domain growth will then follows the non-activated process (domain wall flow motion) and subsequently transforms to the activated process (domain wall creep motion) under the spatially decayed fields. Based on the creep motion formula,  $v \sim \exp(-\alpha/E)$ , the domain radius ( $r$ ) versus pulse duration time ( $t$ ) should follow

$$t - t_0 = \int_{r_0}^r \frac{dr}{v_{\infty} e^{-\alpha/E(r)}} \quad (8)$$

where  $v_{\infty}$  is the upper limit of domain wall speed.  $t_0$  and  $r_0$  are the initial constants and can be considered as the time and domain radius where the domain wall transforms from flow motion to creep motion.  $\alpha$  is the activated field for sidewise domain growth, which is the weighted average of activation fields for the nucleation on the domain wall ( $\alpha_n$ ) and the layered growth of the formed nuclei on the domain wall ( $\alpha_g$ ), i.e.  $\alpha = 1/(n+1)\alpha_n + n/(n+1)\alpha_g$ , where  $n$  is the dimensionality of the domain wall motion<sup>53</sup>.

The derived activation field  $\alpha$  from fitting to the experimental data (Fig. 7b and d) for upward-switching domain growth is about  $372 \text{ MV}/\text{m}$ , while that for the downward-switching domain growth is about  $234 \text{ MV}/\text{m}$ . The higher upward-switching activation field implies that the PVDF/Pt interface lowers the downward polarized domain energy. The average activation field of upward- and downward-switching is about  $303 \text{ MV}/\text{m}$ , which is comparable with the activation field  $\delta$  obtained by the macroscopic measurements. Moreover, the fitted value of  $r_0$  is about  $110\text{--}140 \text{ nm}$  for upward switching voltages from  $-16 \text{ V}$  to  $-20 \text{ V}$ , and about  $160\text{--}200 \text{ nm}$  for downward switching voltages from  $+12 \text{ V}$  to  $+16 \text{ V}$ . These

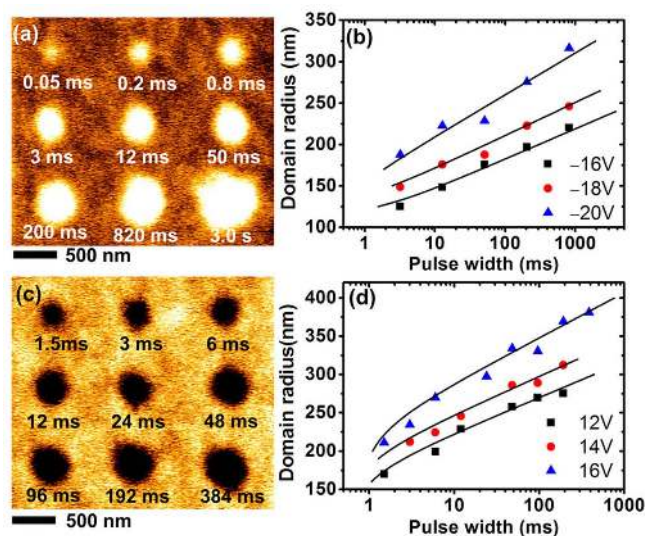


**Figure 7** | PFM study of ferroelectric domains in the P(VDF-TrFE) film. (a) Domains upward switched by tip pulse voltages of  $-18 \text{ V}$  with different pulse durations on a downward polarized matrix. (b) Upward-switched domain radius versus pulse width for tip pulse voltages of  $-16$ ,  $-18$ , and  $-20 \text{ V}$ . (c) Domains downward switched by pulse voltages of  $+14 \text{ V}$  on an upward polarized matrix. (d) Downward-switched domain radius versus pulse width for tip pulse voltages of  $12$ ,  $14$ , and  $16 \text{ V}$ . The solid lines in (b) and (d) are fitting results according to the model of domain wall motion as discussed in the text.



values are higher than those reported for the FE oxide counterparts (about tens of nm)<sup>59,60</sup>.

We also examined the particular arrangement of polarization in the P(VDF-TrFE) films by combining the OP PFM and the in-plane PFM (IP PFM) measurements. The IP PFM signal arises due to the polarization vector  $P$  making an angle of  $\pm 30^\circ$  with the [010] crystallographic axis (b-axis) of the P(VDF-TrFE) crystal<sup>61</sup>. Figure 8 shows the PFM images before and after a square region ( $\sim 500 \times 500 \text{ nm}^2$ ) on the PVDF film was poled by the scanning tip. The tip was biased at  $-10 \text{ V}$  and scanned at a rate of  $1 \text{ Hz}$ . Most OP FE polarization in the as-grown film points toward the bottom substrate, and the switched domains are uniformly poled upward. Due to the domain flow process under the high tip fields, the domain switched region grows beyond the tip writing region which is marked by the dashed line. The IP PFM phase images in Figure 8d before and after the tip poling provide insights on the types of domain switching. The regions where the contrast of IP PFM phase changes suggests  $180^\circ$  dipole rotation along the molecular chains, whereas those unchanged regions can be interpreted as  $120^\circ$  rotation of FE polarization. One typical  $180^\circ$  and one  $120^\circ$  switching regions are highlighted by red and blue circles, respectively. Both types of switching likely proceed through the consecutive events of  $60^\circ$  kink nucleation, especially in the low electric field regime, since the energy barrier of  $60^\circ$  kink nucleation is generally lower than that of  $180^\circ$  kink nucleation<sup>48</sup>.

## Discussion

The classic theory developed by Miller and Weinreich<sup>45,49</sup> proposes that domain wall growth proceeds through the kink nucleation on the walls, conforming to the fact that the switching time usually obeys the Merz' law (equation 5). The more recent models emphasize the pinning effect of defects on the domain wall movements, which leads to the picture of domain wall motions in different creep and viscous flowing modes<sup>8,40</sup>. In this work, we thoroughly checked the issues related to switching dynamics in PVDF polymer films. Despite the distinct features in crystal structure and origin of FE polarization, our data suggest that the polarization switching in PVDF copolymers could be well described by the classic KAI model based on the nucleation and unrestricted domain growth, similar to the fast-switching ceramic counterparts. This is quite remarkable considering the fact that the FE order of P(VDF-TrFE) copolymers hinges on the cooperative long-range rotation of molecular chains via the short-range van der Waals interactions and the intermolecular/interlamella expansion of reversed domains of polarization. As key characteristics

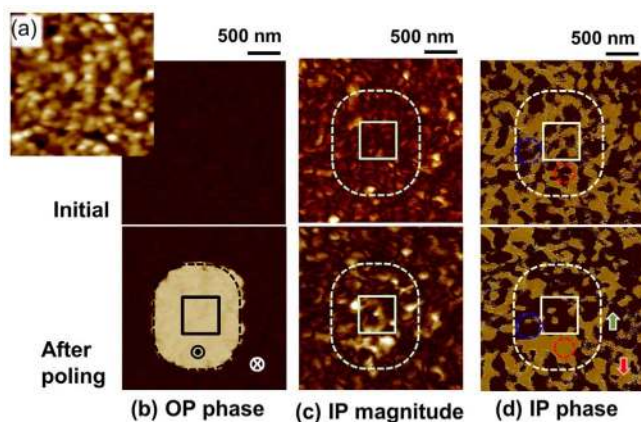


**Figure 8 | Complimentary IP and OP PFM images.** (a) Topography, (b) out-of-plane PFM phase, (c) in-plane PFM magnitude and (d) in-plane PFM phase images taken before and after a region poled by a scanning tip with a bias of  $-10 \text{ V}$ . The solid lines indicate the tip writing region and the dash lines mark the OP switched region. Red and blue circles mark one typical  $180^\circ$  and one  $120^\circ$  switching regions, respectively.

of the kink nucleation at the domain walls, the kink nucleation energy barrier and the domain wall energy at  $300 \text{ K}$  are estimated to be  $29 k_B T$  and  $60 \text{ mJ/m}^2$ , respectively, which are comparable to the values reported for conventional FE ceramics like BTO and PZT.

Using quasi-static  $I(V)$  measurements, we found a lower limit of coercivity  $E_c$  of  $\sim 50 \text{ MV/m}$  at ultra-low frequencies below  $\sim 0.02 \text{ Hz}$ . The lower limit of  $E_c$  suggests the existence of an intrinsic energy barrier for the polarization-switch. If we simply assume that this barrier is associated with a volume with the size of a critical nucleus, it can be simply estimated as  $P \cdot E \cdot V = 0.5 \times 10^{-19} \text{ J}$ . This is close to the energy barrier for nucleation at room temperature ( $29 k_B T = 1.2 \times 10^{-19} \text{ J}$ ), suggesting that this energy barrier is possibly an intrinsic quantity related to the domain nucleation. When the electric field is smaller than  $50 \text{ MV/m}$ , not many nuclei forms and no polarization-switch occurs. This lower threshold coercivity is different with the “intrinsic coercivity” observed for two-dimensional ultrathin LB-PVDF films<sup>25</sup>. The later is believed to be a non-nucleation process which is featured with a huge coercive field of  $\sim 500 \text{ MV/m}$ . The almost independent  $E_c$  on frequency in this low frequency range ( $< 0.01 \text{ Hz}$ ) suggests a very slow relaxation process, which fundamentally differ from the behaviors at higher frequencies.

In addition, we observed crossover between two different scaling regimes of coercivity vs. frequency, which occurs at  $\sim 70 \text{ MV/m}$  and  $100 \text{ Hz}$  at  $300 \text{ K}$ , and the crossover frequency  $f_{cr}$  shifts to lower values on decreasing temperature. Such a crossover phenomenon may be related to the transition of domain wall motions between creep and viscous flow modes. Remarkably, the temperature dependence of crossover features has not been reported before and appears to be unique for P(VDF-TrFE) films. Furthermore, our OP and IP PFM-based switching experiments revealed the existence of both  $180^\circ$  and  $120^\circ$  domains. It is clear that defects act as not only the nucleation centers but also the pinning sites for domain walls in P(VDF-TrFE) polymer films. Overall, our systematic study over wide ranges of temperature and frequency sheds new light on the dynamics of FE switching in PVDF copolymers, bearing implications for the applications of this important class of organic materials.

## Methods

**Materials.** P(VDF-TrFE) (70/30 mol% VDF/TrFE copolymer) films with thickness from  $156 \text{ nm}$  to  $510 \text{ nm}$  were prepared by spin coating. The solutions were first obtained by dissolving P(VDF-TrFE) powders (Piezotech S. A., France) into diethyl carbonate, followed by passing through a PTFE filter with  $0.45 \mu\text{m}$  pore size. The solution was then spin-coated onto Pt(or Cu)(100 nm)/Ti(10 nm)/Si(100) substrates with a speed of  $3000 \text{ RPM}$ . Subsequently, the as-coated film was annealed at  $140^\circ \text{C}$  in air for two hours to improve the crystallinity of the ferroelectric  $\beta$  phase. The thickness of the film was controlled by adjusting the concentration of the solution (from  $1 \text{ w.t.}\%$  to  $8 \text{ w.t.}\%$ ). Finally, the capacitors were prepared by depositing Cu (or Pt) top electrodes with a thickness of  $150 \text{ nm}$  onto the polymer films using thermal evaporation (sputtering) through a shadow mask. The typical size of the top electrodes is  $160 \times 160 \mu\text{m}^2$ .

**Measurements.** The surface morphology and crystallinity of the film was examined by atomic force microscope (AFM, Nanoscope IV, Veeco) and X-ray diffractometer (XRD, Bruker AXS D8 Discover), respectively. Ferroelectric hysteresis loops and switching times were examined by a virtual ground circuit (Radiant Technologies Precision Tester). The samples were cooled down to  $78 \text{ K}$  by nitrogen liquid flowing through a cryogenic micro-manipulated probe station (Janis ST-500-1). The quasi-static  $I(V)$  curves were recorded using a sourcemeter (Keithley 2635A). The nanoscale piezoresponse force microscope (PFM) images were measured using a commercial scanning probe microscope (CPII, Veeco) equipped with a lock-in amplifier. An ac voltage of  $1.0 \text{ V}$  at  $6.39 \text{ kHz}$  was used for modulation.

1. Scott, J. F. & Araujo, C. A. Ferroelectric memories. *Science* **246**, 1400–1405 (1989).
2. Ahn, C. H. *et al.* Local nonvolatile electronic writing of epitaxial  $\text{Pb}(\text{Zr}_{0.52}\text{Ti}_{0.48})\text{O}_3/\text{SrRuO}_3$  heterostructures. *Science* **276**, 1100–1103 (1997).
3. Scott, J. F. Applications of modern ferroelectrics. *Science* **315**, 954–959 (2007).
4. Garcia, V. *et al.* Giant tunnel electroresistance for non-destructive readout of ferroelectric states. *Nature* **460**, 81–84 (2009).
5. Yuan, Y. B. *et al.* Efficiency enhancement in organic solar cells with ferroelectric polymers. *Nat. Mater.* **10**, 296–302 (2011).
6. Lu, H. *et al.* Mechanical writing of ferroelectric polarization. *Science* **336**, 59–61 (2012).





7. Scott, J. F. Nanoferroelectrics: statics and dynamics. *J. Phys. Cond. Matter.* **18**, R361–R386 (2006).
8. Yang, S. M., Yoon, J. G. & Noh, T. W. Nanoscale studies of defect-mediated polarization switching dynamics in ferroelectric thin film capacitors. *Curr. Appl. Phys.* **11**, 1111–1125 (2011).
9. Li, J. *et al.* Ultrafast polarization switching in thin-film ferroelectrics. *Appl. Phys. Lett.* **84**, 1174–1176 (2004).
10. Nelson, C. T. *et al.* Domain dynamics during ferroelectric switching. *Science* **334**, 968–971 (2011).
11. Orihara, H., Hashimoto, S. & Ishibashi, Y. A theory of D-E hysteresis loop based on the Avrami model. *J. Phys. Soc. Jap.* **63**, 1031–1035 (1994).
12. So, Y. W., Kim, D. J., Noh, T. W., Yoon, J. G. & Song, T. K. Polarization switching kinetics of epitaxial Pb(Zr<sub>0.4</sub>Ti<sub>0.6</sub>)O<sub>3</sub> thin films. *Appl. Phys. Lett.* **86**, 092905 (2005).
13. Ishibashi, Y. & Takagi, Y. Note on Ferroelectric Domain Switching. *J. Phys. Soc. Japan* **31**, 506–510 (1971).
14. Tagantsev, A. K., Stolichnov, I. & Setter, N. Non-Kolmogorov-Avrami switching kinetics in ferroelectric thin films. *Phys. Rev. B* **66**, 214109 (2002).
15. Chen, I. W. & Yang, Y. Activation field and fatigue of (Pb,La)(Zr,Ti)O<sub>3</sub> thin films. *Appl. Phys. Lett.* **75**, 4186–4188 (1999).
16. Jung, D. J., Dawber, M., Scott, J. F., Sinnamon, L. J. & Gregg, J. M. Switching dynamics in ferroelectric thin films: An experimental survey. *Integr. Ferroelectr.* **48**, 59–68 (2002).
17. Jo, J. Y. *et al.* Domain switching kinetics in disordered ferroelectric thin films. *Phys. Rev. Lett.* **99**, 267602 (2007).
18. Zhukov, S. *et al.* Dynamics of polarization reversal in virgin and fatigued ferroelectric ceramics by inhomogeneous field mechanism. *Phys. Rev. B* **82**, 014109 (2010).
19. Lovinger, A. J. Ferroelectric polymers. *Science* **220**, 1115–1121 (1983).
20. Ling, Q. D. *et al.* Polymer electronic memories: Materials, devices and mechanisms. *Progress in Polymer Science* **33**, 917–978 (2008).
21. Auciello, O., Scott, J. F. & Ramesh, R. The physics of ferroelectric memories. *Phys. Today* **51**, 22–27 (1998).
22. Horiuchi, S. & Tokura, Y. Organic ferroelectrics. *Nat. Mater.* **7**, 357–366 (2008).
23. Tripathi, A. K. *et al.* Multilevel Information Storage in Ferroelectric Polymer Memories. *Adv. Mater.* **23**, 4146–4151 (2011).
24. Sharma, P., Reece, T. J., Ducharme, S. & Gruverman, A. High-Resolution Studies of Domain Switching Behavior in Nanostructured Ferroelectric Polymers. *Nano Letters* **11**, 1970–1975 (2011).
25. Ducharme, S. *et al.* Intrinsic ferroelectric coercive field. *Phys. Rev. Lett.* **84**, 175–178 (2000).
26. Martinsa, P. P., Lopes, A. C. & Lanceros-Mendez, S. Electroactive phases of poly(vinylidene fluoride): Determination, processing and applications. *Prog. Polym. Sci.* doi:10.1016/j.progpolymsci.2013.07.006.
27. Furukawa, T. Ferroelectric properties of vinylidene fluoride copolymers. *Phase transitions* **18**, 143–211 (1989).
28. Mabuchi, Y., Nakajima, T., Furukawa, T. & Okamura, S. Electric-field-induced polarization enhancement of vinylidene fluoride/trifluoroethylene copolymer ultrathin films. *App. Phys. Exp.* **4**, 071501 (2011).
29. Mao, D., Mejia, L., Stiegler, H., Gnade, B. E. & Quevedo-Lopez, M. A. Polarization behavior of poly(vinylidene fluoride-trifluoroethylene) copolymer ferroelectric thin film capacitors for nonvolatile memory application in flexible electronics. *J. Appl. Phys.* **108**, 094102 (2010).
30. Gysel, R., Stolichnov, I., Tagantsev, A. K., Setter, N. & Mokry, P. Restricted domain growth and polarization reversal kinetics in ferroelectric polymer thin films. *J. Appl. Phys.* **103**, 084120 (2008).
31. Schüttrumpf, J., Zhukov, S., Genenko, Y. A. & Von Seggern, H. Polarization switching dynamics by inhomogeneous field mechanism in ferroelectric polymers. *J. Phys. D: Appl. Phys.* **45**, 165301 (2012).
32. Xu, H. S., Zhong, J. H., Liu, X. B., Chen, J. H. & Shen, D. Ferroelectric and switching behavior of poly(vinylidene fluoride-trifluoroethylene) copolymer ultrathin films with polypyrrole interface. *Appl. Phys. Lett.* **90**, 092903 (2007).
33. Yang, S. M. *et al.* Ac dynamics of ferroelectric domains from an investigation of the frequency dependence of hysteresis loops. *Phys. Rev. B* **82**, 174125 (2010).
34. Karthik, J., Damodaran, A. R. & Martin, L. W. Epitaxial Ferroelectric Heterostructures Fabricated by Selective Area Epitaxy of SrRuO<sub>3</sub> Using an MgO Mask. *Adv. Mater.* **24**, 1610–1615 (2012).
35. Raquet, B., Mamy, R. & Ousset, J. C. Magnetization reversal dynamics in ultrathin magnetic layers. *Phys. Rev. B* **54**, 4128–4136 (1996).
36. Moore, T. A. & Bland, J. A. C. Mesofrequency dynamic hysteresis in thin ferromagnetic films. *J. Phys.: Condens. Matter.* **16**, R1369 (2004).
37. Kleemann, W. Annu. Universal Domain Wall Dynamics in Disordered Ferroic Materials. *Rev. Mater. Res.* **37**, 415–448 (2007).
38. Nattermann, T., Pokrovsky, V. & Vinokur, V. M. Hysteretic Dynamics of Domain Walls at Finite Temperatures. *Phys. Rev. Lett.* **87**, 197005 (2001).
39. Sharma, P., Nakajima, T., Okamura, S. & Gruverman, A. Effect of disorder potential on domain switching behavior in polymer ferroelectric films. *Nanotech.* **24**, 015706 (2013).
40. Tybell, T., Paruch, P., Giamarchi, T. & Triscone, J. M. Domain Wall Creep in Epitaxial FerroelectricPb(Zr<sub>0.2</sub>Ti<sub>0.8</sub>)O<sub>3</sub> Thin Films. *Phys. Rev. Lett.* **89**, 097601 (2002).
41. Cao, W. & Krumhansl, J. Continuum theory of 4 mm-2 mm proper ferroelastic transformation under inhomogeneous stress. *Phys. Rev. B* **42**, 4334–4340 (1990).
42. Viehland, D. & Chen, Y. H. Random-field model for ferroelectric domain dynamics and polarization reversal. *J. Appl. Phys.* **88**, 6696–6707 (2000).
43. Yin, J. H. & Cao, W. W. Coercive field of 0.955Pb(Zn<sub>1/3</sub>Nb<sub>2/3</sub>)O<sub>3</sub>-0.045PbTiO<sub>3</sub> single crystal and its frequency dependence. *Appl. Phys. Lett.* **80**, 1043–1045 (2002).
44. Merz, W. J. Domain formation and domain wall motions in ferroelectric BaTiO<sub>3</sub> single crystals. *Phys. Rev.* **95**, 690–698 (1954).
45. Miller, R. C. & Savage, A. Further experiments on the sidewise motion of 180° domain walls in BaTiO<sub>3</sub>. *Phys. Rev.* **115**, 1176–1180 (1959).
46. Scott, J. F. *et al.* Switching kinetics of lead zirconate titanate submicron thin-film memories. *J. Appl. Phys.* **64**, 787–792 (1988).
47. Nakajima, T., Abe, R., Takahashi, Y. & Furukawa, T. Intrinsic switching characteristics of ferroelectric ultrathin vinylidene fluoride/trifluoroethylene copolymer films revealed using Au electrode. *Jap. J. Appl. Phys.* **44**, L1385 (2005).
48. Aharon, H. D., Sluckin, T. J. & Taylor, P. L. Kink propagation as a model for poling in poly(vinylidene fluoride). *Phys. Rev. B* **21**, 3700–3707 (1980).
49. Miller, R. C. & Weinreich, G. Mechanism for the sidewise motion of 180° domain walls in Barium Titanate. *Phys. Rev.* **117**, 1460–1466 (1960).
50. Jiang, A. Q., Lee, H. J., Hwang, C. S. & Scott, J. F. Sub-picosecond processed of ferroelectric domain switching from field and temperature experiments. *Adv. Func. Mater.* **22**, 192–199 (2012).
51. Nakhmanson, S. M., Nardelli, M. B. & Bernholc, J. Collective polarization effects in β-polyvinylidene fluoride and its copolymers with tri- and tetrafluoroethylene. *Phys. Rev. B* **72**, 115210 (2005).
52. Jo, J. Y. *et al.* Polarization switching dynamics governed by thermodynamic nucleation process in ultrathin ferroelectric films. *Phys. Rev. Lett.* **97**, 247602 (2006).
53. Shin, Y. H., Grinberg, I., Chen, I. W. & Rappe, A. M. Nucleation and growth mechanism of ferroelectric domain-wall motion. *Nature* **449**, 881–884 (2007).
54. Kalinin, S. V., Morozovska, A. N., Chen, L. Q. & Rodriguez, B. J. Local polarization dynamics in ferroelectric materials. *Rep. Prog. Phys.* **73**, 056502 (2010).
55. Jesse, S. *et al.* Direct imaging of the spatial and energy distribution of nucleation centres in ferroelectric materials. *Nat. Mater.* **7**, 209–215 (2008).
56. Morozovska, A. N. *et al.* Local polarization switching in the presence of surface-charged defects: Microscopic mechanisms and piezoresponse force spectroscopy observations. *Phys. Rev. B* **78**, 054101 (2008).
57. Kim, Y. *et al.* Non-Kolmogorov-Avrami-Ishibashi Switching Dynamics in Nanoscale Ferroelectric Capacitors. *Nano Lett.* **10**, 1266–1270 (2010).
58. Kim, Y. *et al.* Universality of Polarization Switching Dynamics in Ferroelectric Capacitors Revealed by 5D Piezoresponse Force Microscopy. *Adv. Funct. Mater.* **23**, 3971–3979 (2013).
59. Chen, Y. C. *et al.* Non-volatile domain nucleation and growth in multiferroic BiFeO<sub>3</sub> films. *Nanotech.* **22**, 204030 (2011).
60. Chen, Y. C., Lin, Q. R. & Chu, Y. H. Domain growth dynamics in single-domain-like BiFeO<sub>3</sub> thin films. *Appl. Phys. Lett.* **94**, 122908 (2009).
61. Sharma, P., Wu, D., Poddar, S., Reece, T. J. & Ducharme, S. Orientational imaging in polar polymers by piezoresponse force microscopy. *J. Appl. Phys.* **110**, 052010 (2011).

## Author contributions

W.J.H., Y.H.C. and T.W. conceived and designed the experiments. W.J.H., D.M.J., L.Y. and Y.C.C. carried out the experiments. W.J.H. and T.W. wrote the paper. All authors discussed the results and commented on the manuscript.

## Additional information

**Competing financial interests:** The authors declare no competing financial interests.

**How to cite this article:** Hu, W.J. *et al.* Universal Ferroelectric Switching Dynamics of Vinylidene Fluoride-trifluoroethylene Copolymer Films. *Sci. Rep.* **4**, 4772; DOI:10.1038/srep04772 (2014).



This work is licensed under a Creative Commons Attribution-NonCommercial-NoDerivs 3.0 Unported License. The images in this article are included in the article's Creative Commons license, unless indicated otherwise in the image credit; if the image is not included under the Creative Commons license, users will need to obtain permission from the license holder in order to reproduce the image. To view a copy of this license, visit <http://creativecommons.org/licenses/by-nc-nd/3.0/>